A Non-simultaneous Dynamic Ice-structure Interaction Model

Xu Ji*, Dale G. Karr**, Erkan Oterkus***

* Department of Naval Architecture, Ocean and Marine Engineering, University of Strathclyde
100 Montrose Street, Glasgow, G4 0LZ, United Kingdom
Phone: +44 (0)141 5484094
e-mail: x.ji@strath.ac.uk

** Department of Naval Architecture and Marine Engineering, University of Michigan
2600 Draper Drive, Ann Arbor, Michigan, 48109, United States of America
Phone: +1 (734) 764-3217
e-mail: dgkarr@umich.edu

*** Department of Naval Architecture, Ocean and Marine Engineering, University of Strathclyde
100 Montrose Street, Glasgow, G4 0LZ, United Kingdom
Phone: +44 (0)141 5483876
e-mail: erkan.oterkus@strath.ac.uk

Abstract:
To simulate non-simultaneous ice failure effects on ice-structure interaction, an extended dynamic Van der Pol based numerical model is developed. The concept of multiple ice failure zones is proposed to fulfil non-simultaneous crushing characteristics. Numerical results show that there is more simultaneous force acting on all segments at lower ice velocity and there is more non-simultaneous ice failure at higher velocity. Variations of force records show a decreasing trend with increasing ice velocity and structural width. These effects can be attributed to the assumption that the size of ice failure zone becomes smaller with increasing ice velocity, which increases the occurrence of non-simultaneous ice failures. Similarly, the decreasing size of ice failure zone as velocity increases is explained as the reason of different ice failure modes shifting from large-area ductile bending to small-area brittle crushing. The simulation results from a series of 134 demonstration cases show that the model is capable of predicting results at different ice velocities, structural widths and ice thicknesses. In addition, analysis of the ice indentation experiments indicates that the mean and minimum effective pressure have an approximately linear relationship with ice velocity, which testified the assumption on variations of ice failure zone in the model.

Keywords:
Non-simultaneous failure; Ice-structure interaction; Ice failure zone; Van der Pol equation.

NOMENCLATURE

L_i	Ice failure length of each ice strip (m)
c	Constant distributed normally with mean μ and variance σ_s^2
H	Ice thickness (m)
v_0	Reference velocity (m s^{-1})
v	Ice velocity (m s^{-1})

K_0	Reference stiffness (kN m^{-1})
K	Structural stiffness (kN m^{-1})
N_{strip}	Number of ice strips
W_i	Width of an ice failure zone (m)
M	Mass of the structure (kg)
C	Damping coefficient (kg s^{-1})
ξ	Damping ratio
$\ddot{X}$	Structural acceleration (m s^{-2})
$\dot{X}$	Structural velocity (m s^{-1})
X	Structural displacement (m)
T	Time (s)
A	Magnification factor
σ	Ice stress (kPa)
D	Structural width (m)
q_i	Dimensionless fluctuation variable of each ice strip
a, ε	Scalar parameters that control the q_i profile
ω_i	Angular frequency of ice force (rad s^{-1})
f_i	Ice failure frequency (Hz)
B	Coefficient depending on ice properties
$\dot{Y}_i$	Velocity of each ice strip (m s^{-1})
Y_i	Displacement of each ice strip (m)
$\ddot{Y}_i$	Acceleration of each ice strip (m s^{-2})
$\sigma_{\max}$	Maximum stress at ductile-brittle range (kPa)
σ_d, σ_b	Minimum stress at ductile and brittle range (kPa)
v_r	Relative velocity between ice and structure (m s^{-1})
v_t	Transition ice velocity approximately in the middle of transition range (m s^{-1})
α, β	Positive and negative indices to control the envelope profile
μ_P	Mean effective pressure (kPa)
σ_P	Standard deviation of effective pressure (kPa)
F_μ	Mean value of ice force (kN)
F_σ	Standard deviation of ice force (kN)
$\Delta\mu_p$, $\Delta\sigma_p$	The difference between the results from model and experiment for μ_p and σ_p

1. INTRODUCTION

As the study of ice failure has advanced, non-simultaneous failure has gained increasing attention. It can be utilized to explain several well-recognized issues, such as higher localized pressure zone than global pressure (Johnston et al., 1998) and different failure modes at different indentation speeds (Sodhi and Haehnel, 2003).

Kry (1978) proposed an estimation of statistical influence on non-simultaneous failure across a wide structure and divided the ice interaction surface into multiple equivalent zones that are statistically independent of each other. Then Kry (1980) found that ice generally had a more uniform contact with a structure at low velocity and more irregular contact at higher velocity. Ashby et al. (1986) explained the non-simultaneous failure as a size effect resulting from cracks of different lengths having been distributed statistically in ice. Bhat (1990) proposed that ice fails at many self-similar zones like many other fractals in nature and proposed an equation to control the size effect depending on the scale to estimate the irregular ice contact geometry.

Sodhi (1998) used segmented indentors to conduct a series of ice indentation tests and found simultaneous failure at low velocity and non-simultaneous at high velocity, and proposed an equation to estimate the decreasing size of ice failure length with increasing indentation velocity. Yue et al. (2009) installed ice load panel on a full-scale monopod platform and found simultaneous ice failure on different panels during lock-in condition.

At the same time, many ice-structure interaction numerical models have been developed. Matlock et al. (1971) proposed the very first ice-structure interaction model and many Matlock based numerical models have been developed since then (Huang and Liu, 2009; Karr et al., 1993; Withalm and Hoffmann, 2010). Non-simultaneous ice-structure interaction models have been developed based on Matlock model (Hendrikse et al., 2011; Yu and Karr, 2014) by extending the single ice strip into multiple strips moving towards the structure. Another method of modelling the interaction process is through utilizing Van der Pol ice force oscillator to control ice force fluctuations (Wang and Xu, 1991). Three distinctive structural response modes and ice-induced vibration phenomenon were captured in Ji and Oterkus (2016). Physical mechanism of ice-structure interaction at each stage were discussed based on feedback mechanism and energy mechanism in Ji and Oterkus (2018).

In this study, following the concept of Matlock-based non-simultaneous modeling, an extension of Ji and Oterkus (2018) Van der Pol based model is introduced. Apart from the ice velocity and structural stiffness effect on the ice failure, a normally distributed variable is added in the ice failure length equation instead of a constant in the previous model. In addition, the previous one-dimensional single strip ice model is extended to a two-dimensional multiple strips ice model in this study.

2. EXPERIMENTAL DATA FROM SODHI (1998)

Sodhi (1998) listed 159 test results including structural width D, ice thickness H, ice velocity v, mean μ_p and standard deviation σ_p of the effective pressure across the interaction surface. In Test 582 and 576 as well as Test 764 and 763, they are sharing similar ice thickness and structural width but different ice velocities. In Test 582 and 764 as well as Test 576 and 763, they share similar velocities but different ice thicknesses and structural widths. Therefore, different tests, Test. 582, 576, 764 and 763, are simulated by the numerical model. The time history of ice force and structural displacement are plotted and compared with the time history of experimental results.

To use the data more efficiently for blind test later, they are relisted in the Table 1. There are four main sections in total with different D ranging from 50 mm, 150 mm, 250 mm to 350 mm. Each section has several groups of data from (A) to (K). Each group has the ice thickness with 1 mm difference, or rarely with 1.5mm difference. Then each group is sorted from the lowest to the highest ice velocity. There are 25 tests that are not grouped together because of limited similar ice thickness, as shown in grey color in the Table 1. Therefore, 134 different tests are simulated by only changing the D, H and v. Then, μ_p and σ_p are compared between the numerical simulations and experimental results.

Table 1. Test configurations from Sodhi (1998).

Test	D mm	H mm	v mm s^{-1}	μ_p MPa	σ_p MPa	Group
166	50	25.1	62	2.032	0.243	
160	50	27.3	80	2.307	0.34	
165	50	24.8	100	2.12	0.224	
167	50	25	125	1.78	0.291	
164	50	26.3	199	1.504	0.319	**(A)**
163	50	25.6	300	1.644	0.256	
162	50	26.3	400	1.622	0.263	
161	50	25.7	492	1.915	0.301	
158	50	45.1	47	1.736	0.229	
154	50	44.4	82	1.681	0.229	
153	50	45.2	101	1.548	0.237	
155	50	44.2	127	1.877	0.265	
156	50	43.3	156	1.417	0.307	
157	50	43.5	188	1.394	0.408	**(B)**
152	50	45.6	197	1.461	0.188	
159	50	45.3	224	1.363	0.25	
151	50	43.9	304	1.392	0.247	
150	50	45.6	393	1.497	0.231	
175	50	69.7	103	2.491	0.555	
176	50	71.1	136	2.509	0.742	
362	150	15.3	406	2.405	0.275	
388	150	18.8	10	1.62	0.634	
387	150	18.8	20	0.806	0.25	
378	150	18.7	25	0.925	0.288	
386	150	18.5	31	1.086	0.306	
385	150	18.5	42	0.856	0.239	
377	150	18.7	42	0.986	0.287	
376	150	18.7	42	0.91	0.266	
373	150	17.3	52	1.012	0.192	
375	150	17.6	74	1.055	0.192	**(C)**
374	150	17.6	90	0.915	0.36	
375	150	17.6	99	1.144	0.199	
371	150	17.8	100	1.114	0.177	
372	150	17.8	200	1.263	0.171	
369	150	18.5	391	1.462	0.147	
370	150	18	394	1.399	0.167	
368	150	18.5	469	1.508	0.178	
384	150	19.2	21	0.991	0.331	
403	150	24.5	14	2.083	0.769	
402	150	24.5	21	1.657	0.724	
401	150	25.5	31	0.99	0.344	

Test	D mm	H mm	v mm s^{-1}	μ_p MPa	σ_p MPa	Group
399	150	25.5	44	0.933	0.3	
398	150	26.6	20	1.69	0.906	
391	150	27	20	1.907	0.862	
390	150	27	45	1.029	0.347	
410	150	30.6	20	1.869	0.831	
405	150	30	27	2.214	0.967	
411	150	30	43	1.077	0.321	
404	150	30	43	1.265	0.45	
356	150	32.3	81	1.402	0.4	
354	150	32.8	97	1.665	0.544	**(D)**
358	150	31.8	134	1.374	0.357	
357	150	32.4	134	1.372	0.287	
361	150	30.5	181	1.424	0.231	
359	150	31.2	187	1.178	0.245	
353	150	32.7	197	1.62	0.236	
351	150	33.3	395	2.06	0.197	
352	150	33.4	294	1.813	0.223	
366	150	45.1	194	1.706	0.38	
367	150	46	270	1.959	0.231	
364	150	46.2	197	1.819	0.45	
363	150	46.8	301	2.186	0.236	
534	250	17.9	48	0.803	0.287	
536	250	17.8	56	0.874	0.226	
535	250	17.7	72	0.864	0.207	
537	250	18.1	72	0.834	0.384	
538	250	17.9	73	0.917	0.167	
533	250	18	102	0.893	0.2	
521	250	18.2	149	0.997	0.13	**(E)**
532	250	18.1	201	1.026	0.184	
540	250	18.1	249	1.123	0.121	
531	250	18.2	300	1.158	0.212	
539	250	18.1	350	1.257	0.135	
549	250	18.5	355	1.234	0.13	
548	250	18.4	499	1.319	0.161	
516	250	24.8	10	1.58	0.948	
513	250	24.8	10	1.454	0.597	
528	250	25.4	21	1.536	0.791	
514	250	24.6	42	0.934	0.382	**(F)**
527	250	25.4	42	1.025	0.421	
592	250	23.6	83	0.937	0.253	
590	250	24.1	104	1.003	0.195	

Test	D mm	H mm	v mm s^{-1}	μ_p MPa	σ_p MPa	Group
591	250	23.8	159	1.055	0.157	
589	250	23.9	202	1.141	0.131	
593	250	24	254	1.181	0.116	
588	250	24	315	1.212	0.132	
587	250	24.5	373	1.246	0.121	**(F)**
586	250	24.7	408	1.304	0.115	
585	250	25.1	465	1.377	0.124	
583	250	25.7	490	1.611	0.127	
582	250	32.7	102	0.961	0.288	
579	250	33.9	133	1.085	0.214	
578	250	33.3	199	1.199	0.162	
572	250	34.6	199	1.25	0.277	
581	250	33	246	1.236	0.146	
577	250	34.2	312	1.291	0.141	**(G)**
580	250	33	356	1.32	0.132	
575	250	33.2	386	1.436	0.131	
569	250	34.7	400	2.067	0.169	
576	250	33.9	409	1.383	0.129	
545	250	35.8	110	0.917	0.2	
596	250	35.1	200	1.194	0.169	
546	250	36.3	200	1	0.372	
544	250	35.6	215	1.065	0.147	
543	250	35.9	277	1.207	0.146	
547	250	36.8	298	1.238	0.362	**(H)**
595	250	35.4	301	1.41	0.17	
571	250	35.9	304	1.462	0.145	
542	250	35.5	331	1.332	0.145	
541	250	35.9	375	1.315	0.141	
594	250	35.5	399	1.581	0.182	
554	250	41.5	6	1.732	1.033	
555	250	42	6	1.572	1.419	
551	250	41.1	8	1.006	1.327	
559	250	40.4	145	1.197	0.29	
525	250	41.3	201	1.453	0.491	
563	250	39.8	300	1.503	0.514	**(I)**
524	250	40.9	304	1.77	0.256	
526	250	40.9	353	1.926	0.157	
523	250	39.8	392	2.112	0.179	
522	250	40.1	467	1.992	0.231	

Test	D mm	H mm	v mm s^{-1}	μ_p MPa	σ_p MPa	Group
556	250	42.2	6	1.258	0.807	
560	250	43.1	219	1.289	0.182	
553	250	44.3	8	1.198	0.819	
552	250	44.3	8	1.38	1.02	
760	350	20.3	82	0.835	0.143	
752	350	22.2	100	0.899	0.174	
759	350	20.2	156	0.939	0.088	
761	350	20.5	157	0.915	0.105	
755	350	20.7	172	0.994	0.094	
758	350	20.2	251	1.001	0.095	**(J)**
754	350	20.8	306	1.125	0.093	
757	350	20.3	354	1.117	0.085	
753	350	20.8	401	1.17	0.089	
751	350	21.1	453	1.214	0.09	
756	350	20.4	459	1.163	0.082	
771	350	24.5	80	0.859	0.263	
773	350	23.8	99	0.898	0.219	
777	350	24.5	99	1.121	0.298	
764	350	25.2	100	1.015	0.341	
779	350	24.8	115	1.067	0.278	
770	350	23.9	121	1.029	0.108	
780	350	24.8	150	1.223	0.217	
781	350	24.9	157	1.197	0.124	
782	350	25	193	1.23	0.122	
766	350	24.6	196	1.11	0.111	**(K)**
772	350	24	197	1.143	0.11	
776	350	24.5	199	1.272	0.133	
769	350	23.9	248	1.23	0.128	
775	350	24.7	277	1.547	0.123	
765	350	24.8	303	1.194	0.099	
768	350	24.4	350	1.264	0.099	
774	350	24.4	358	1.371	0.129	
767	350	24.4	452	1.297	0.105	
762	350	25.6	481	1.598	0.104	
763	350	26.4	401	1.405	0.105	
785	350	29.8	198	1.273	0.134	
784	350	30	305	1.624	0.129	
783	350	30.4	399	1.503	0.121	

To show the ice velocity effect on the ice force level, four groups of data, (C), (E), (F) and (J) at different structural widths with similar ice thickness are selected from Table 1, as shown in Figure 1. Figure 1 (a) and (b) show the mean μ_p and standard deviation σ_p of the effective pressure from the Table 1, respectively. Figure 1 (c) and (d) are the maximum and minimum effective pressure calculated from $\mu_p \pm 2\sigma_p$, respectively. In Figure 1 (a) and (c), the pressure decreases from higher value to the lowest value first before ice velocity reaches the transition ice velocity. Reason of this pressure difference can be the difference between static frictional force at low velocity and kinetic frictional force at high velocity (Ji and Oterkus, 2018). After the transition ice velocity, the mean value increases approximately linearly with increasing ice velocity. It is due to the fact that there is more momentum energy transferred to the structure from ice, i.e. higher acceleration of the structure in the form of $F = M(\partial v/\partial T)$. Apart from ice speed effect, it shows that thicker ice has higher effective pressure and wider structure has lower effective pressure. In other words, the higher the aspect ratio of structural width D over ice thickness H, the lower the effective pressure is.

Figure 1 (b) shows the standard deviation of pressure decreases with increasing velocity. The decreasing trend indicates smaller ice failure size and the occurrence of more non-simultaneous failure. Provided that the minimum effective pressure to be $\mu_p - 2\sigma_p$, Figure 1 (d) also indicates that it has more dependency on ice velocity and less dependency on structural width or ice thickness. Slope at lower velocity is higher since simultaneous failure has large standard deviation caused by the maximum force value. For the same reason, the data points at lower velocity calculated in this method has less accuracy. Because there should not be any of negative pressure. Then the minimum value increases approximately linearly with ice velocity, which means that the lower bound of ice force follows the similar pattern. Considering that most part of the ice maintains constant contact with structure at high ice speed after failure, ice force will not reduce back to zero as that at lower ice speed.

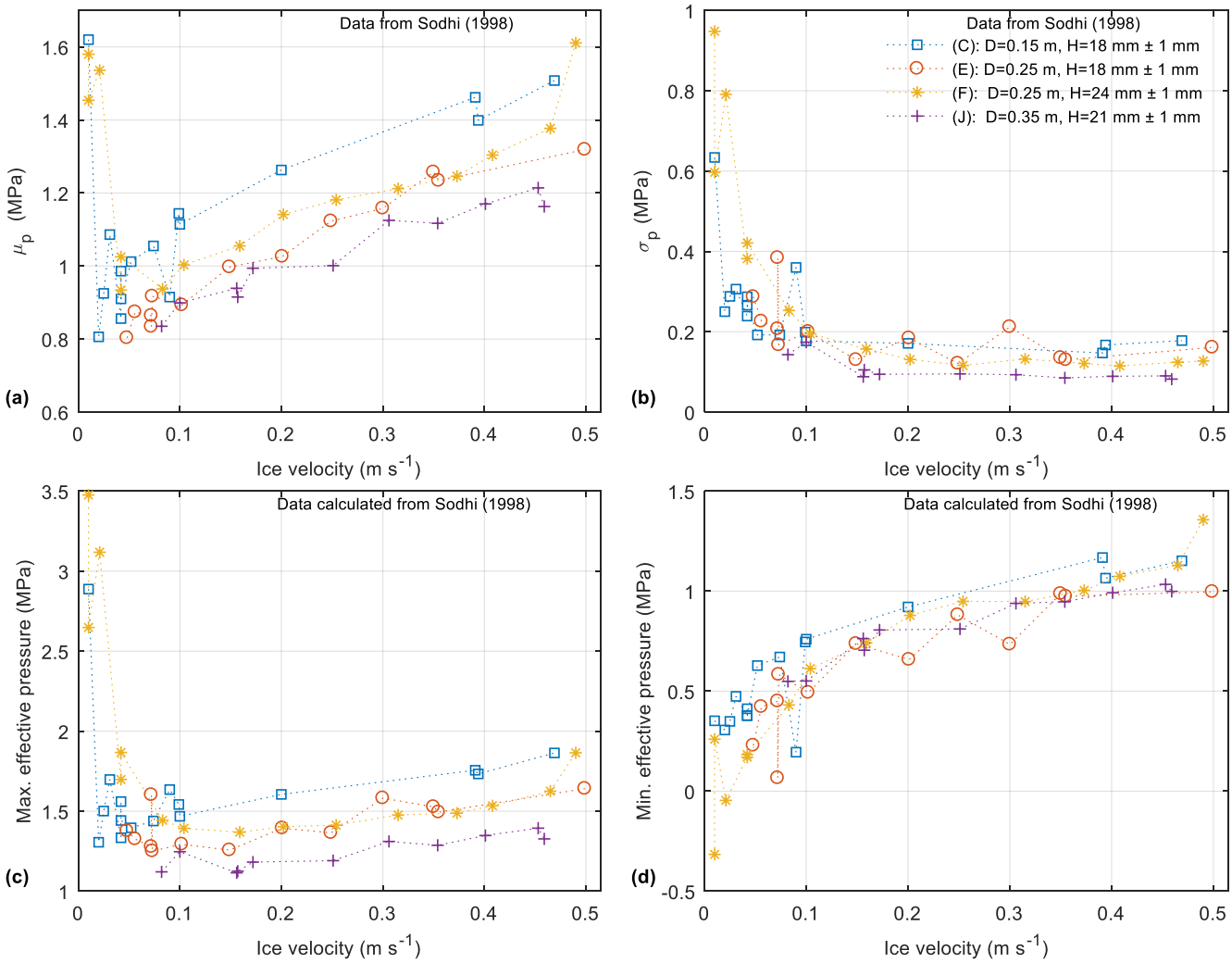

Fig. 1. Ice velocity vs. the (a) mean, (b) standard deviation, (c) maximum and (d) minimum of effective pressure from the data group of (C), (E), (F) and (J) in Table 1.

3. MODEL DESCRIPTION

3.1 Ice failure zone

The governing equations in the model proposed here are mainly adopted from Ji and Oterkus (2018). There are some improvements between the previous work and the current one. The previous ice failure length, $L = 2H(v_0 / v)(K_0 / K)$, in the single ice strip model with different structural rigidities and ice velocities were justified in Ji and Oterkus (2018). The constant of 2, as Sodhi used, was in the range of 1-3 in the experiment. Therefore, c is assumed to follow a normal relationship in the range of 1-3. As shown in Figure 2, the ice sheet is modeled as multiple strips moving towards a mass-spring-damper idealized structure. Each ice strip is assumed to be independent of each other and fails at a normally distributed random length of L_i, as specified in Eq. (1)

$$L_i = cH(v_0 / v)(K_0 / K) \tag{1}$$

where L_i is the ice failure length of each strip, c is a variable distributed normally in the form of $c \sim N(\mu, \sigma_s^2)$ with mean μ and variance σ_s^2, v_0 is the reference velocity, v is the ice velocity, K_0 is the reference stiffness and K is the structural stiffness.

As shown in the Figure 1 (b), the decreasing standard deviation is related with the decreasing size of ice failure zone. Therefore, it is presumed that ice sheet fails at smaller ice failure zones with higher ice speed with the dimension of $L_i \times W_i \times H$, as illustrated in Figure 1, where the width of an ice failure zone W_i is equal to the structural width D over the number of ice strips, i.e. $W_i = D/N_{strip}$. Besides a decreasing ice failure length with increasing ice speed relationship, the width W_i is also assumed to be inversely proportional to the ice velocity v. In other words, the number of ice strips N_{strip} is proportional to ice velocity v, as specified in Eq. (2), which means that there are more ice strip failure across the interaction surface as the ice speed increases,

$$N_{strip} = (20v+1)N_{seg} \tag{2}$$

where N_{seg} is the corresponding number of segments in Sodhi's experiment and each segment has a width of 50 mm, i.e. N_{seg}= 1, 3, 5, 7 at D= 50, 150, 250 ,350 mm, respectively. The constant 20 is calibrated based on the comparison between numerical and experimental results and the N_{strip} should be round up to an integer during calculation in the case of a decimal value.

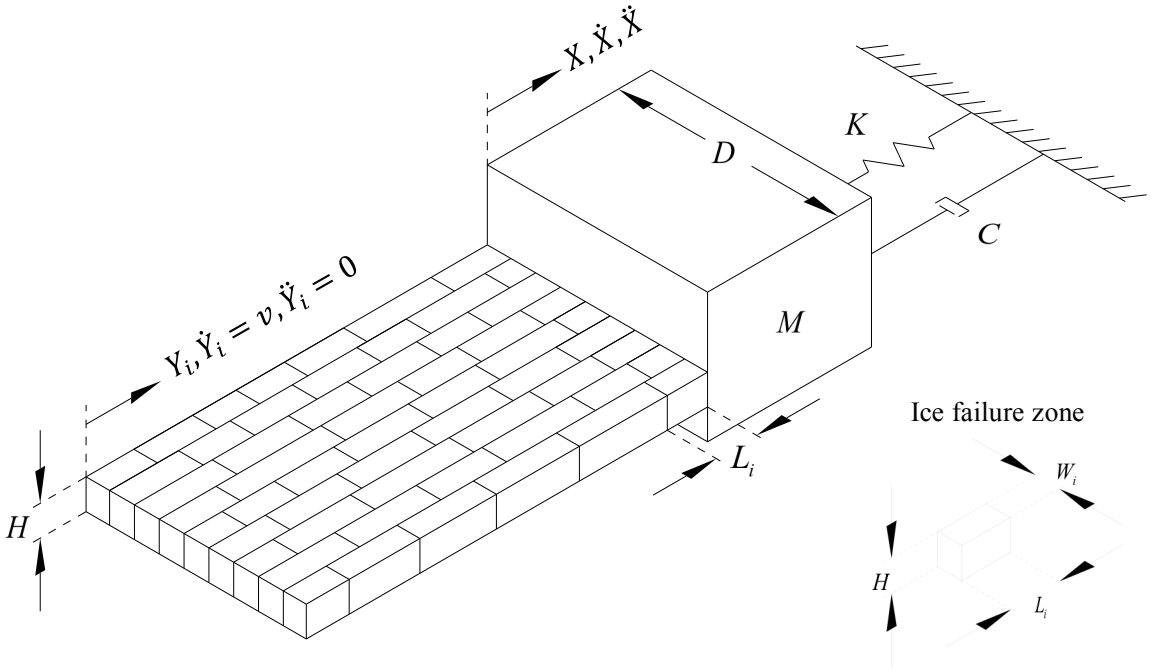

Fig. 2. Schematic sketch of non-simultaneous dynamic ice-structure model.

3.2 Governing equations

In this study, compared with the model in Ji and Oterkus (2018), the ice sheet is extended to multiple strips for non-simultaneous failure characteristics in Eq. (3) and (4). Each ice failure zone applies a local ice force to the structure that is controlled by the product of area and stress and the variable q_i from Van der Pol oscillator equation adjusted by a magnification factor A. By adding up each local ice force, the total ice force will result in the structure to vibrate in a single degree-of-freedom first-mode motion. The Van der Pol equation is an oscillator with non-linear damping to describe the saw-tooth ice force fluctuation characteristic. There are internal and external effects regarding the oscillator in Eq. (4). Internal effect is an assumption that ice has its own original failure characteristic length which corresponds to the oscillator without relative velocity related forcing term on the right-hand side of the oscillator equation. By considering internal effect only, the ice failure frequency can be calculated using the relationship $f_i = v / L_i$. External effect corresponds to structural

effects including structural displacement and structural velocity, i.e. relative displacement and relative velocity between ice and structure. Relative velocity takes effect in the forcing term of the Van der Pol oscillator and ice strain rate-stress function in Eq. (6). Relative displacement reflects to compressive stress resulting in ice deformation and when the deformation exceeds the ice failure length L_i, ice failure occurs. Therefore, each ice failure zone will fail under both internal and external effects.

$$MX + CX + KX = \sum_{i=1}^{N_{strip}} AHW_i\sigma(q_i + a) \tag{3}$$

$$q_i + \varepsilon\omega_i(q_i^2 - 1)q_i + \omega_i^2 q_i = \frac{B\omega_i}{H}(Y_i - X) \tag{4}$$

In Eq. (3) and Eq. (4), M is the mass of the structure, X is the displacement of the structure, the "dot" symbol represents the derivative with respect to time T, C is the damping coefficient, A is the magnification factor for oscillator variable adjusted from experimental data, H is the ice thickness, σ is the variable ice stress satisfying Eq. (6), N_{strip} is the number of ice strips, q_i is the dimensionless fluctuation variable of each ice strip, a and ε are scalar parameters that control the lower bound of ice force value and saw-tooth ice force profile, respectively. Since Figure 1 (d) shows that the minimum effective pressure increases with increasing velocity, the lower bound a is assumed to increase linearly with ice velocity, as specified in Eq. (5), where the coefficients are calibrated based on the comparison between numerical and experimental results for Test. 582, 576, 764 and 763.

$$a(v) = 7v + 4/3 \tag{5}$$

$\omega_i = 2\pi f_i$ is the angular frequency of each ice strip force at each particular ice failure length, $f_i = v / L_i$ is the frequency of each ice strip force, B is a coefficient depending on ice properties and Y_i is the displacement of each ice strip. In conjunction with the ice stress power functions (Huang and Liu, 2009),

$$\sigma = \begin{cases} (\sigma_{\max} - \sigma_d)(v_r / v_t)^{\alpha} + \sigma_d, & v_r / v_t \le 1 \\ (\sigma_{\max} - \sigma_b)(v_r / v_t)^{\beta} + \sigma_b, & v_r / v_t > 1 \end{cases} \tag{6}$$

where $\sigma_{\max}$ is the maximum stress at ductile-brittle range, σ_d and σ_b are the minimum stress at ductile and maximum stress at brittle range, respectively, α and β are positive and negative indices to control the envelope profile, respectively, and v_t is the transition ice velocity approximately in the middle of transition range. Further and justification of the parameters are provided in detail in the next section.

3.3 Parameter values

The parameters in Eq. (1-4) and Eq. (6) are determined and calibrated by the experimental results summarized in Sodhi (1998). The mass of the structure $M = 600$ kg and damping ratio $\xi = 0.1$ are found in the earlier experimental configuration in Sodhi (1991). Ice velocity, ice thickness, structural stiffness and structural width are directly used from the Table 1. Values of A, a, ε and B are used directly from Ji and Oterkus (2018). K_0, α and β are adjusted by the preliminary simulation results from Test. 582 and Test. 576. Stress variations range is approximately from 1.6 MPa to 4.5 MPa and there is a clear boundary between higher and lower stress value at the velocity of 0.03 m s^{-1}. Therefore, $v_t = 0.03$ m s^{-1}, $\sigma_{\min} = 1600$ kPa and $\sigma_{\max} = 4500$ KPa are used for the minimum and maximum stress, respectively. As suggested in Sodhi (1998), $v_0 = 0.03$ m s^{-1} and c varies between 1 to 3. Therefore, the mean value is set to $\mu = 2$ and standard deviation is $\sigma_s = 0.3$. A summary of parameter values is listed below:

$M = 600$ kg, $\xi = 0.1$, $K = 35000$ kN m^{-1}, $A = 0.19$, $\varepsilon = 4.6$, B = 0.1;
$\sigma_d = 2000$ kPa, $\sigma_b = 1600$ kPa, $\sigma_{\max} = 4500$ kPa, $\alpha = 0.5$, $\beta = -0.7$, $v_t = 0.03$ m s^{-1};
$v_0 = 0.03$ m s^{-1}, $K_0 = 10000$ kN m^{-1}, $\mu = 2$, $\sigma_s = 0.3$.

4. RESULTS AND DISCUSSION

Based on the experimental results summarized in Table 1, four different tests, Test. 582, 576, 764 and 763, are considered. To differentiate the number of numerical simulation and the experimental test, the reproduced numerical results from the corresponding tests are named after STest. and with the corresponding test number, i.e. numerical simulation STest. 582 for experimental Test. 582. Results obtained from the current numerical model are shown in Figures 3-6. Each figure contains time history plot of total ice force, ice force on each segment and structural displacement. Comparison between numerical results and experiments shows quantitively agreement with the envelope profile of all forces and structural displacement. The mean value F_μ and standard deviation F_σ of ice force are listed in Table 2, in which the force is calculated by the product of interaction area and effective pressure. The difference between the results from the model and experiment for F_μ and F_σ, i.e. ΔF_μ and ΔF_σ, are also listed to show the error rate of results.

Table 2. Results from experimental tests and numerical simulations.

No.	Test.		STest.		ΔF_μ	ΔF_σ
	F_μ (kN)	F_σ (kN)	F_μ (kN)	F_σ (kN)		
582	7.856	2.354	7.77	2.675	-1.10%	13.62%
576	11.721	1.093	11.712	0.904	-0.08%	-17.31%
764	8.952	3.008	8.875	2.914	-0.86%	-3.11%
763	12.982	0.970	12.438	0.822	-4.19%	-15.28%

Although force records in Figure 3 and 4 are showing non-simultaneous characteristic in general, there are still different levels of simultaneousness if only one cycle of failure is considered. Force records in STest. 582 show that there is occurrence of a sudden peak force on all segments simultaneously, resulting in large amplitude of force upon the structure, whereas peak force occurs randomly in STest. 764 upon different segments of the structure.

The pattern of smaller variations and higher mean value of ice force with increasing ice velocity coincide with the test results, as shown in Figure 3 and 5 as well as Figure 4 and 6. However, as Sodhi mentioned, variations of ice force should decrease when structural width becomes larger, as in STest. 576 and STest.763 shown in Figure 5 and 6, respectively. On the contrary, both numerical and test results from Test. 764 and STest.764 have higher standard deviation than that from Test. 582 and STest. 582. The reason is that figures in Sodhi (1998) are just plotted in one second. Moreover, the starting and ending time in those figures are not picked at the same time period which makes the statistics less accurate. Because of the randomness in the numerical model, the occurrence and quantity of those four typical ice forces would appear randomly at both STest. 582 and STest. 764. This means that the randomness would exist in the real experiment.

Moreover, it can be noticed that there is more non-simultaneous failure in STest. 764 (Figure 4) than that in STest. 582 (Figure 3) and in STest. 763 (Figure 6) than STest. 576 (Figure 5), respectively. Due to increasing ice speed and structural width, the size of ice failure zone becomes smaller, i.e. the number of ice failure zone increases. Hence, the possibility of non-simultaneous failure increases and variation of ice force decreases. Similarly, ice-velocity effect on the size of ice failure zones can also be the reason of different ice failure

modes at different speeds. As the size of ice failure zone decreases with increasing ice speed, ice will fail from larger size to smaller size, which corresponds to the ductile bending mode to brittle crushing mode, respectively. Technically, a cycle of simultaneous ice failure will reduce back to zero value entirely after the unloading phase. There are two reasons of this lower bound of ice force variations. One is attributed to the non-simultaneous characteristic where there are some ice zones remaining in contact with the structure before failure occurs. The other is purely physical contact with the structure leading to high level of ice force.

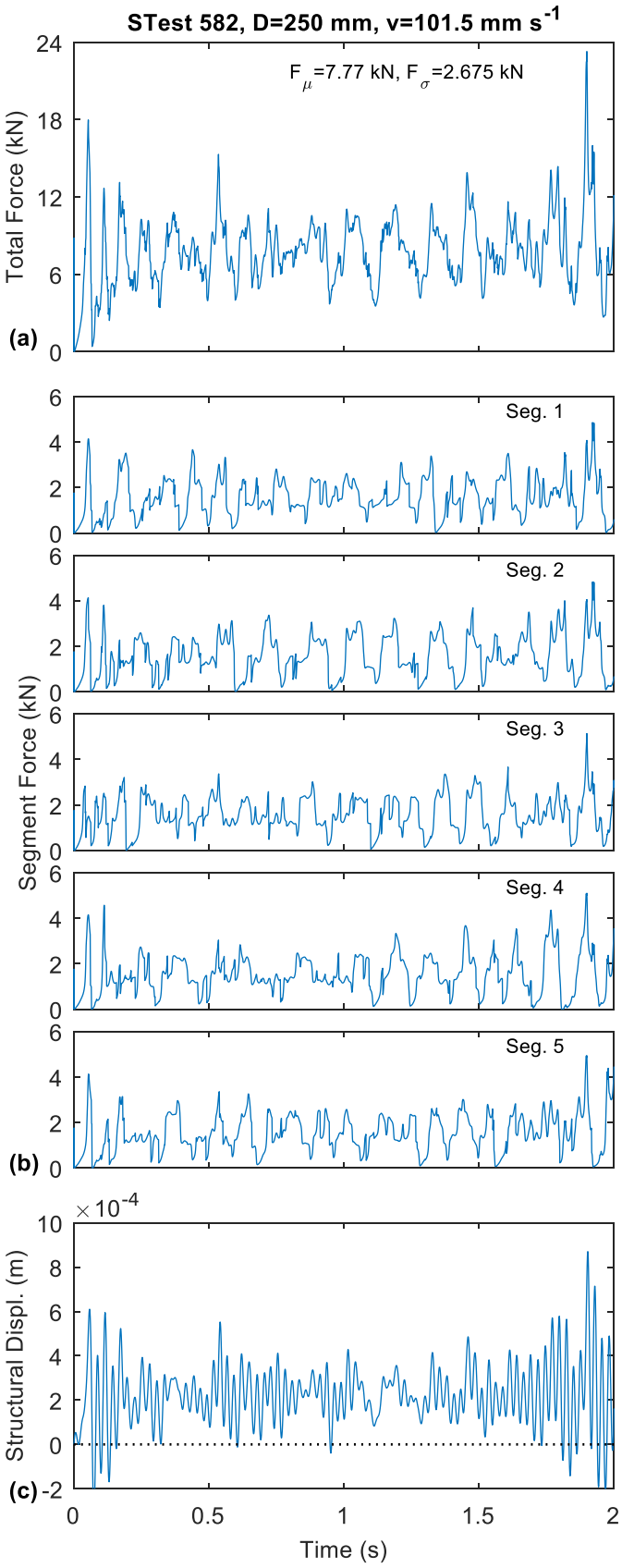

Fig. 3. Time history of (a) total ice force; (b) ice force on each segment; (c) structural displacement with 5 segments at D= 250 mm, v= 101.5 .m s^{-1}.

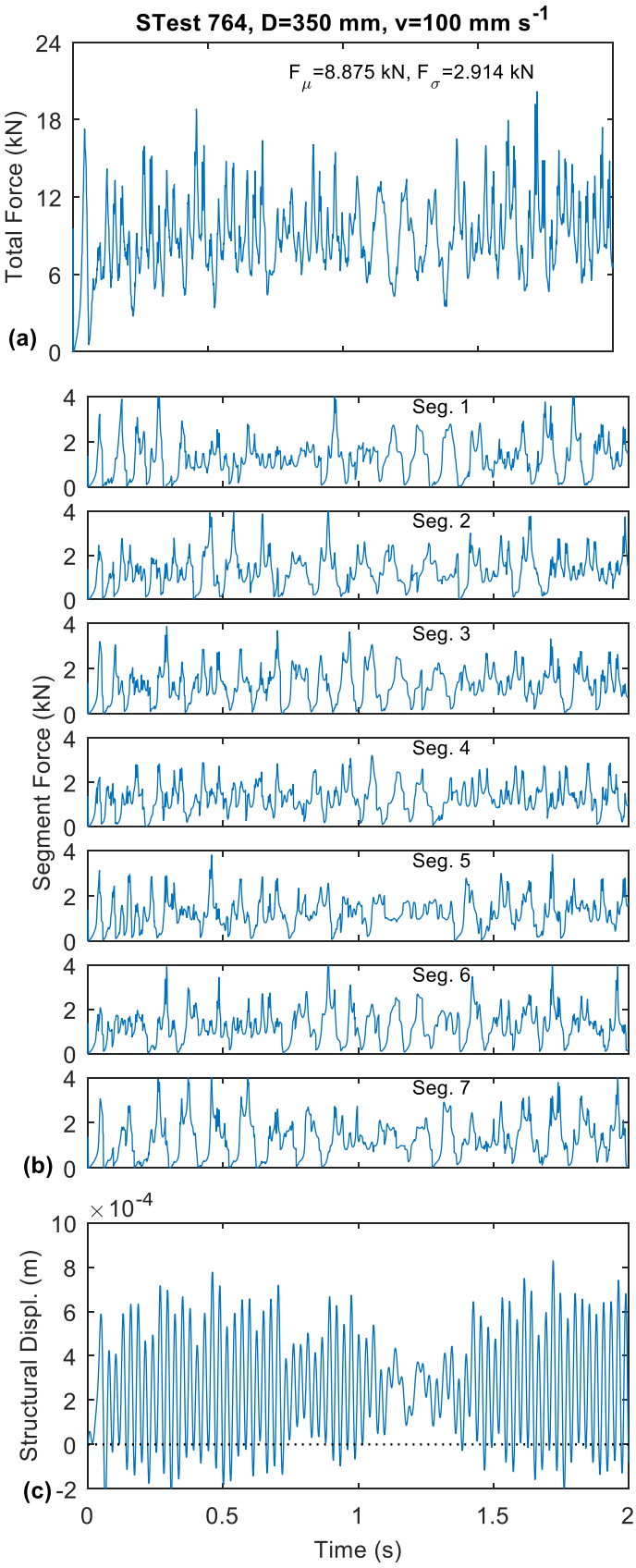

Fig. 4. Time history of (a) total ice force; (b) ice force on each segment; (c) structural displacement with 7 segments at D= 350 mm, v= 100 mm s^{-1}.

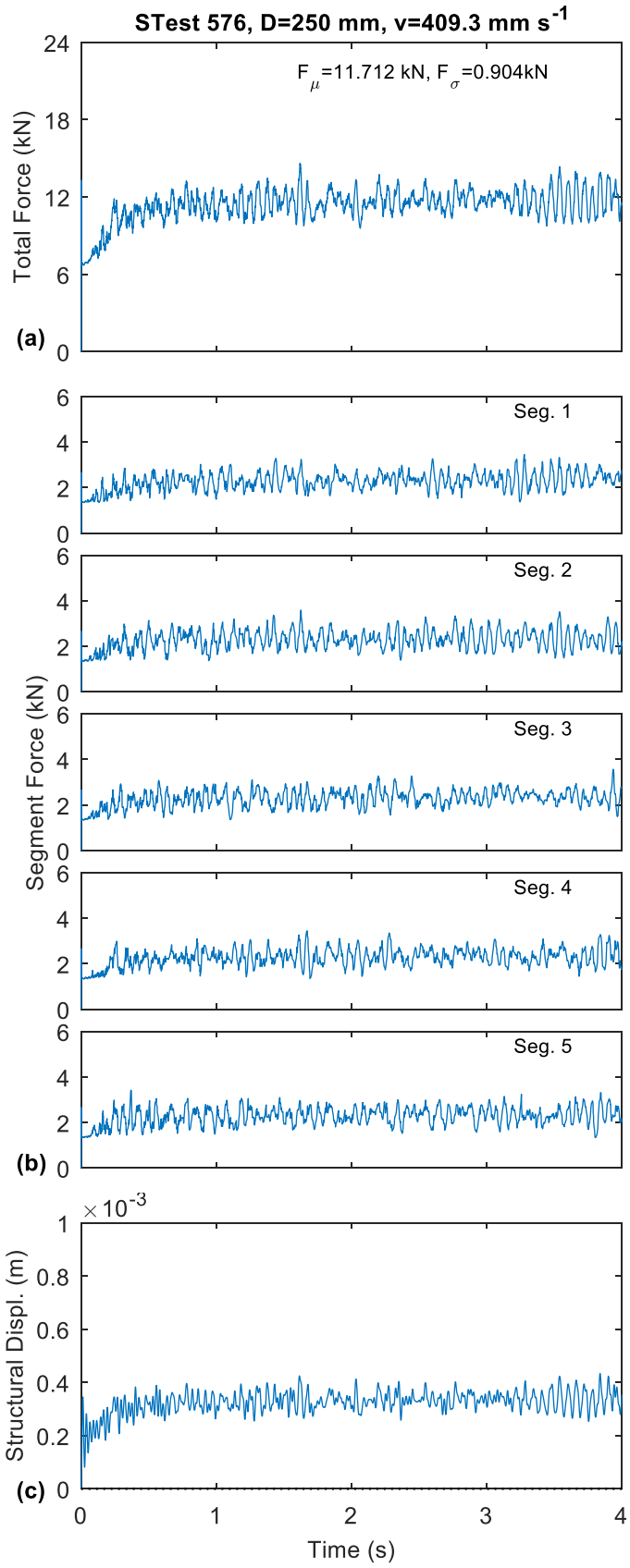

Fig. 5. Time history of (a) total ice force; (b) ice force on each segment; (c) structural displacement with 5 segments at D= 250 mm, v= 409.3 mm s^{-1}.

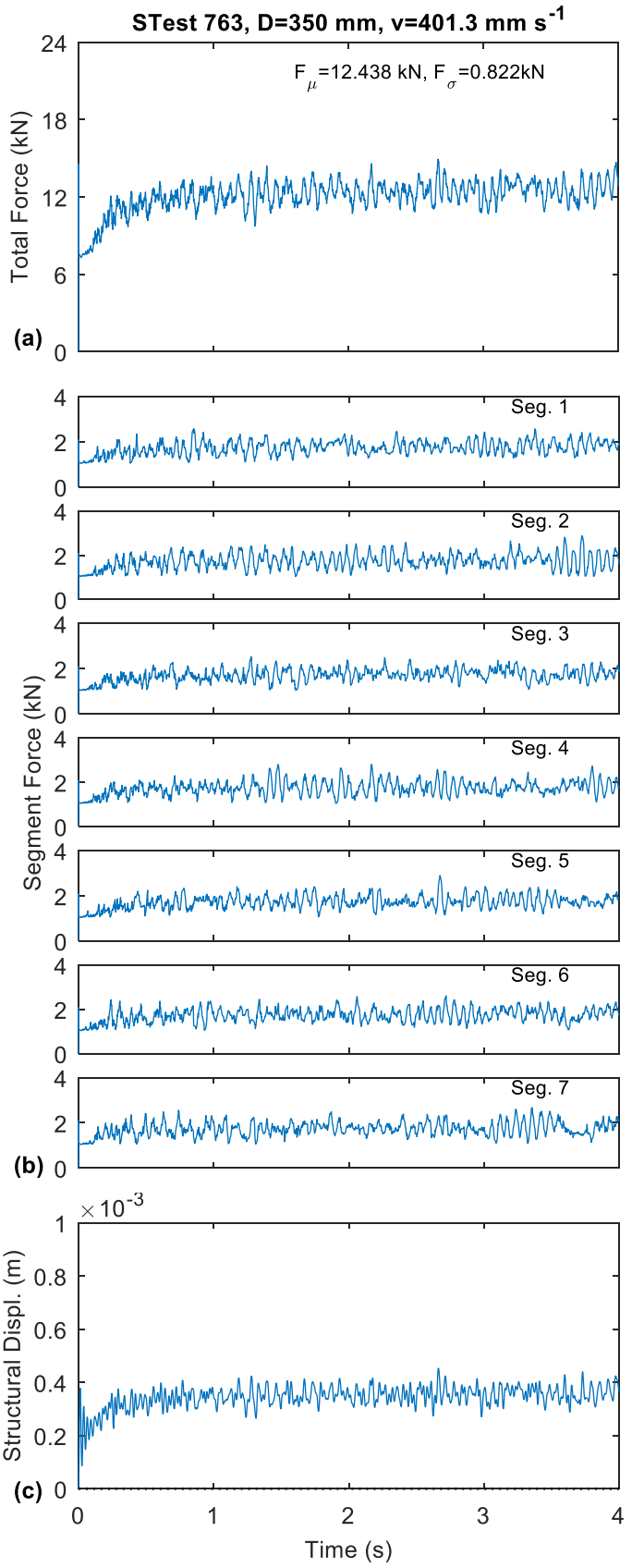

Fig. 6. Time history of (a) total ice force; (b) ice force on each segment; (c) structural displacement with 7 segments at D= 350 mm, v= 401.3 mm s^{-1}.

5. DEMOSTRATION CASES

To test the calibrated model's capability at different D, H and v, it is used to simulate 134 different tests from Group (A) to (K) in Table 1. Same configurations as those in the previous four simulations are used by only changing the D, H and v. Figure 7 (a-k) show a series of comparisons of μ_p and σ_p between the model (plotted in red) and experiment (plotted in blue) as the ice velocity increases. The model captures the general trend of μ_p and σ_p as v increases, especially at some fluctuation points. Meanwhile, there are some abnormal experimental results that require a double-check, such as the peak points in Figure 7 g(1) and h(2). The μ_p and σ_p has better accuracy as the ice velocity increases, as shown in Figure 8. The difference between the results from model and experiment for μ_p and σ_p, i.e. $\Delta\mu_p$ and $\Delta\sigma_p$, are plotted against v with the mean of -6.05% and 11.42% difference, respectively.

Figure 9 shows the histogram of the $\Delta\mu_p$ and $\Delta\sigma_p$ with an interval of 10% between each bar. The number on the top of each bar shows the corresponding percentage weighted among all data. The model can predict well on the mean value that 76.8% of data yields a value within the 20% of difference between the model and experiment. In terms of σ_p, 71% of data yields a value within the 50% of difference and 30.7% of data yields a value within the 20% of difference. The less accuracy at lower velocity range can be the reason of corresponding ductile ice failure property. The failure mechanism in the numerical model is supposed to simulate the crushing brittle ice failure behavior, in which ice fails at certain amount of length.

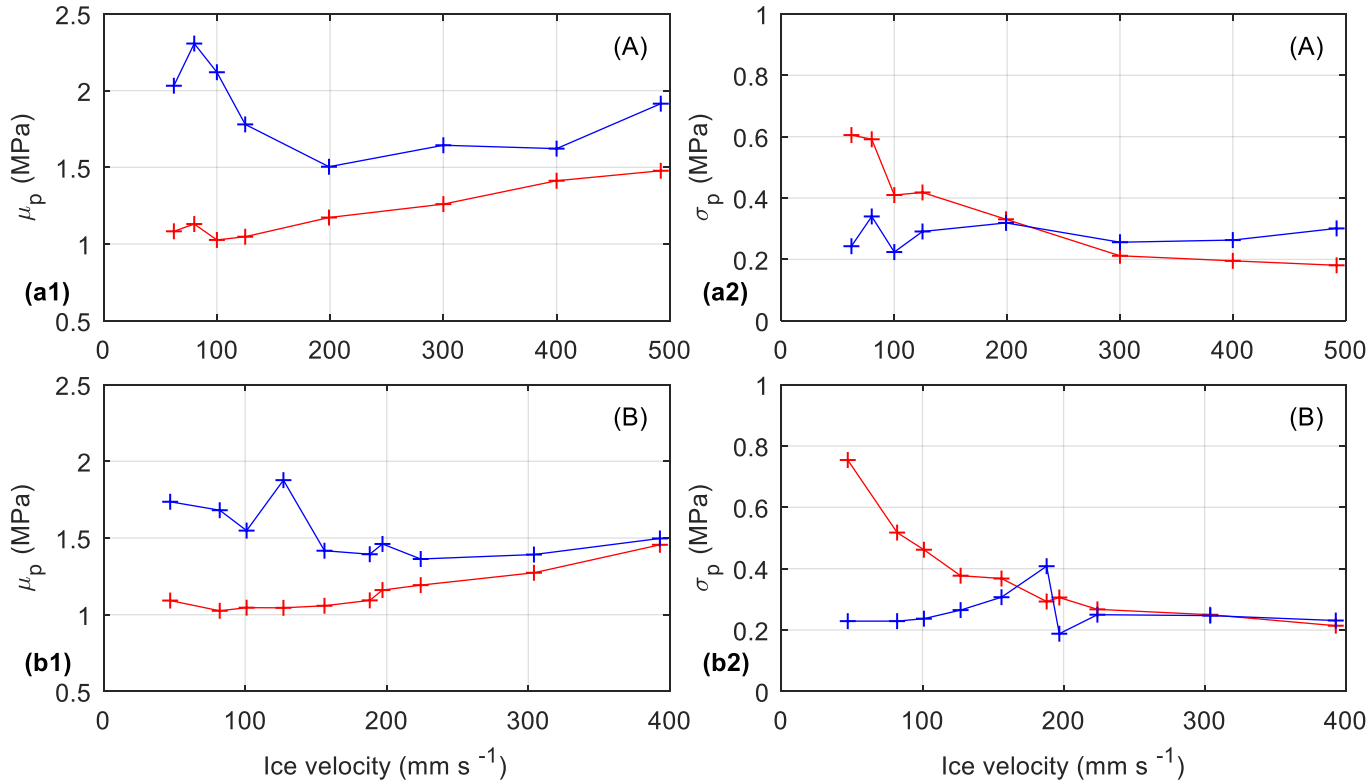

Fig. 7. (a-b) *D*=50 mm.

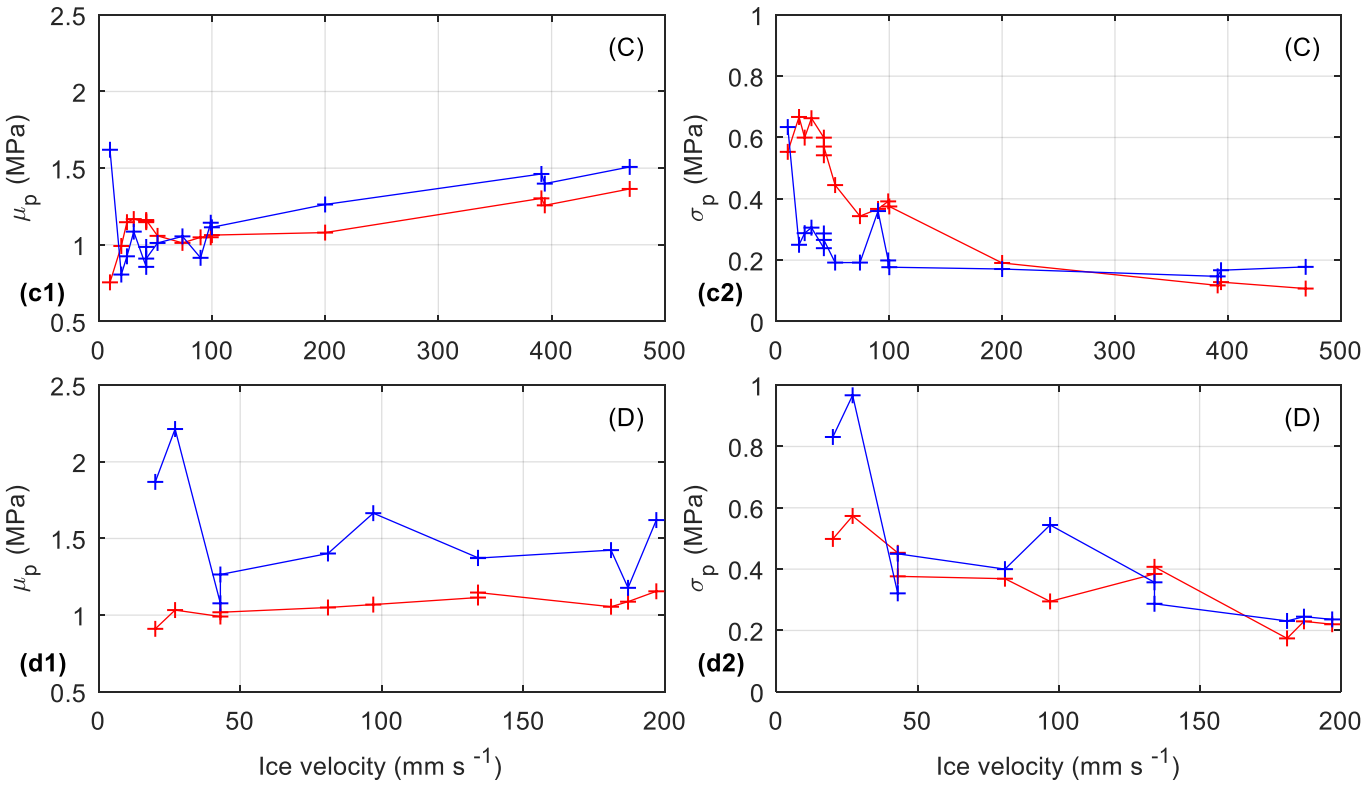

Fig. 7. (c-d) D =150 mm.

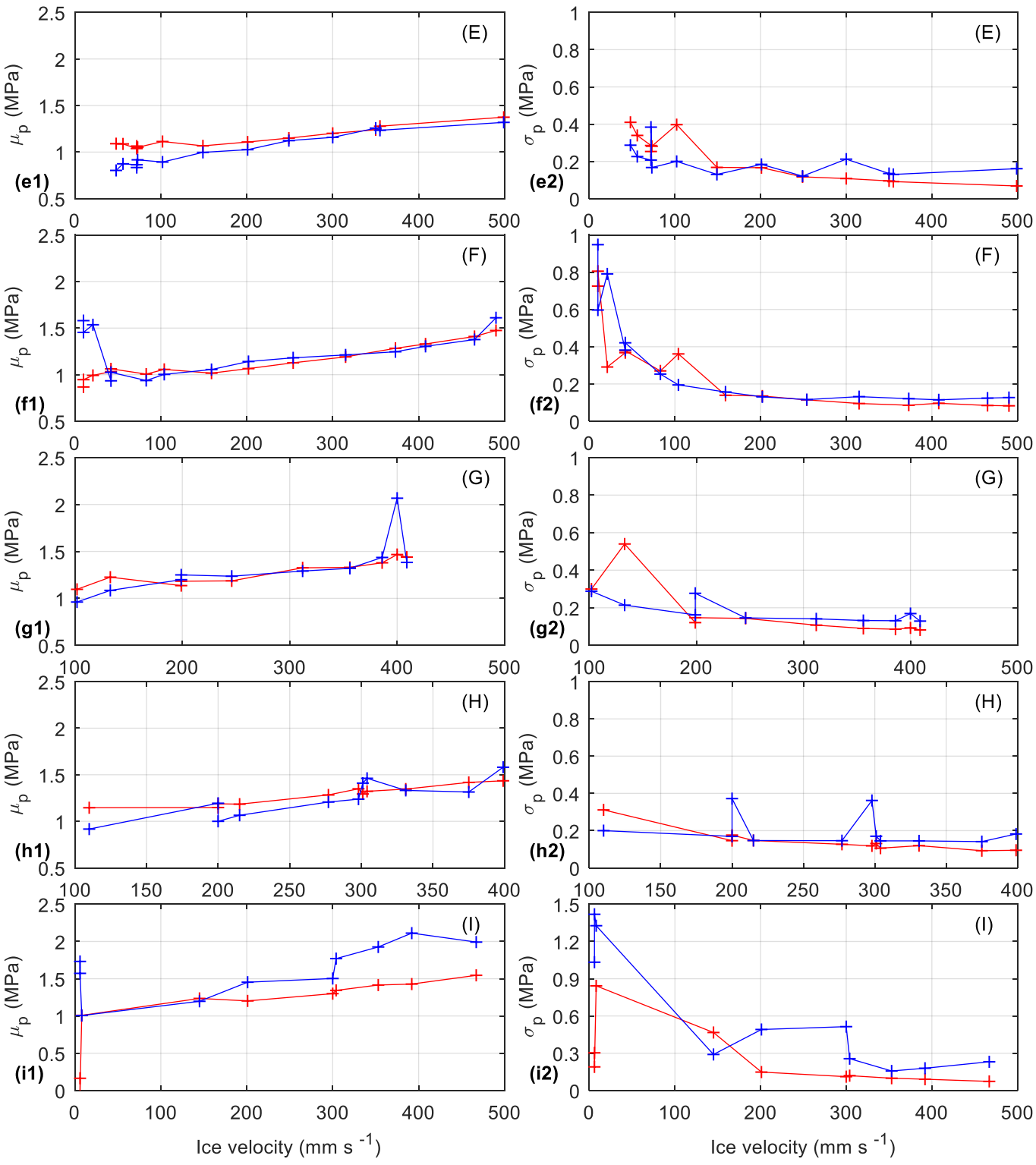

Fig. 7. (e-i) D =250 mm.

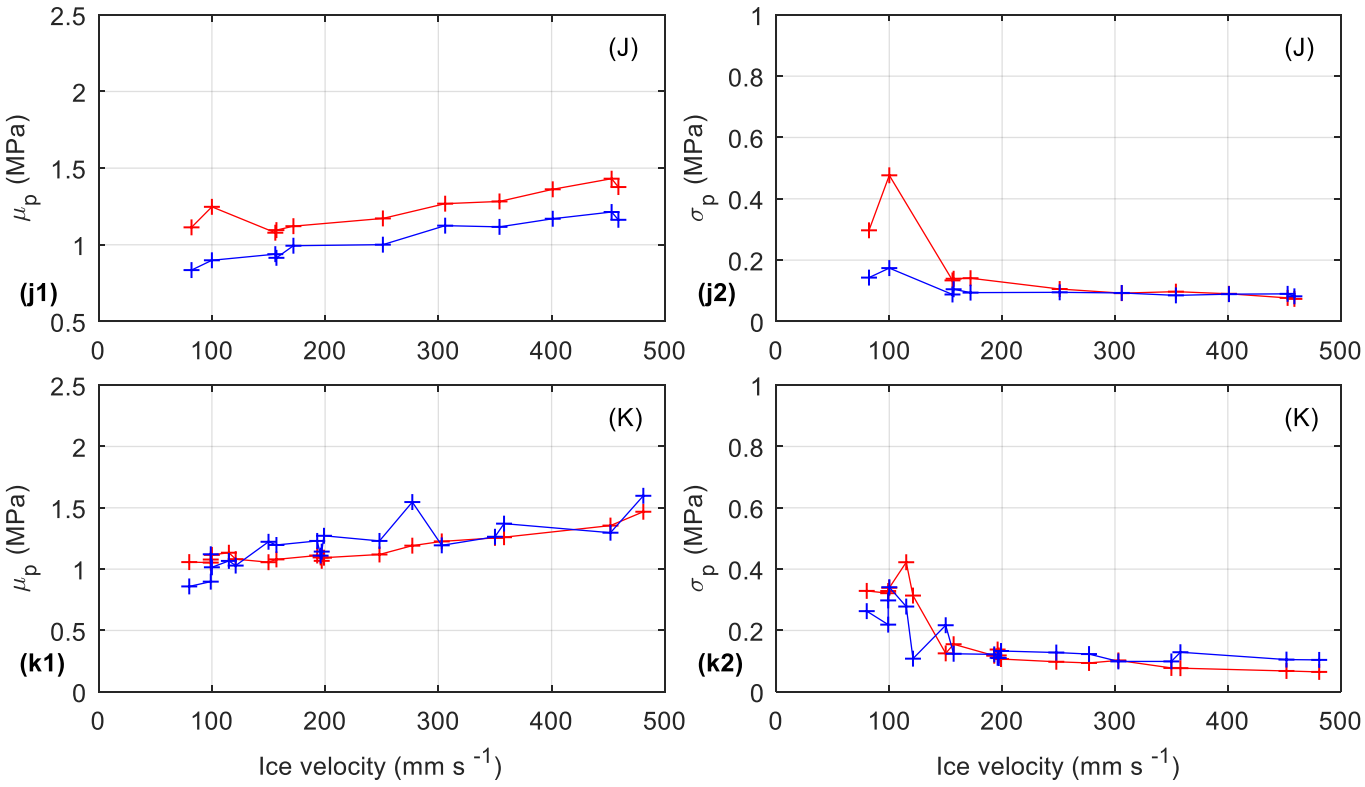

Fig. 7. Ice velocity vs. the mean μ_p and standard deviation σ_p of the effective pressure across the interaction surface from numerical simulations (red line) and experimental results (blue line), at (a-b) D=50 mm, (c-d) D =150 mm, (e-i) D =250 mm, (j-k) D =350 mm with the corresponding data group of (A) to (K) from Table 1.

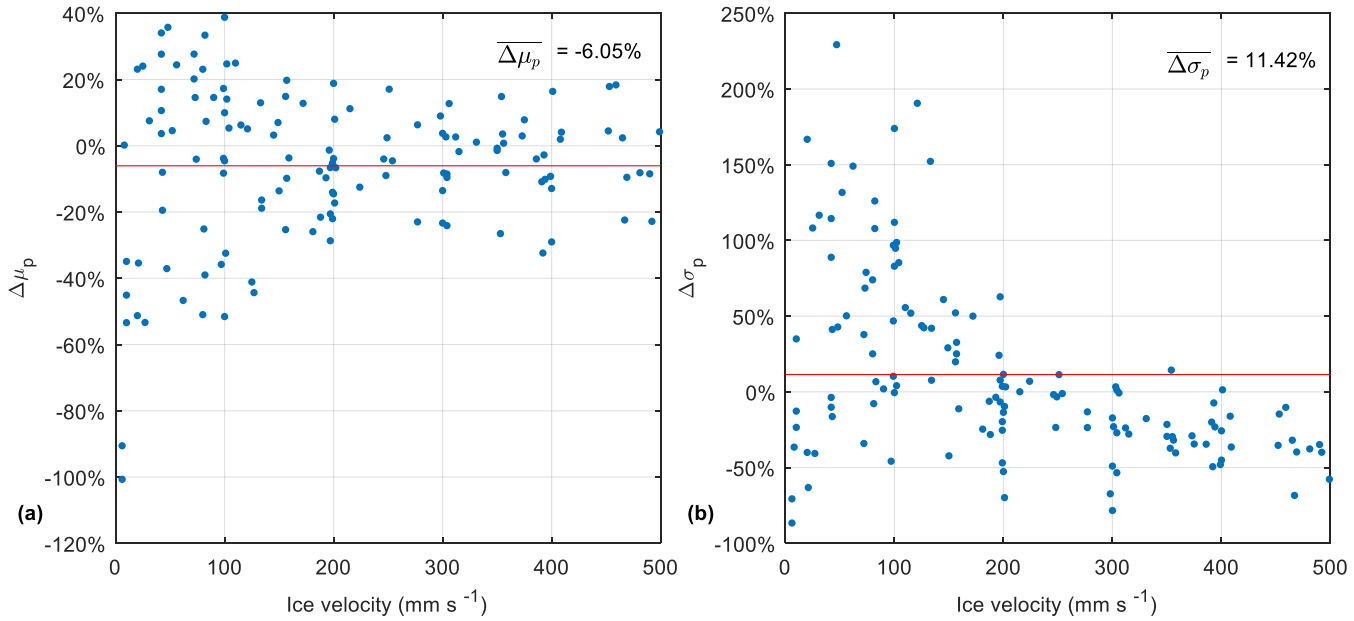

Fig. 8. Ice velocity vs. (a) mean and (b) standard deviation of the effective pressure difference (in percentage) between numerical simulations and experimental results.

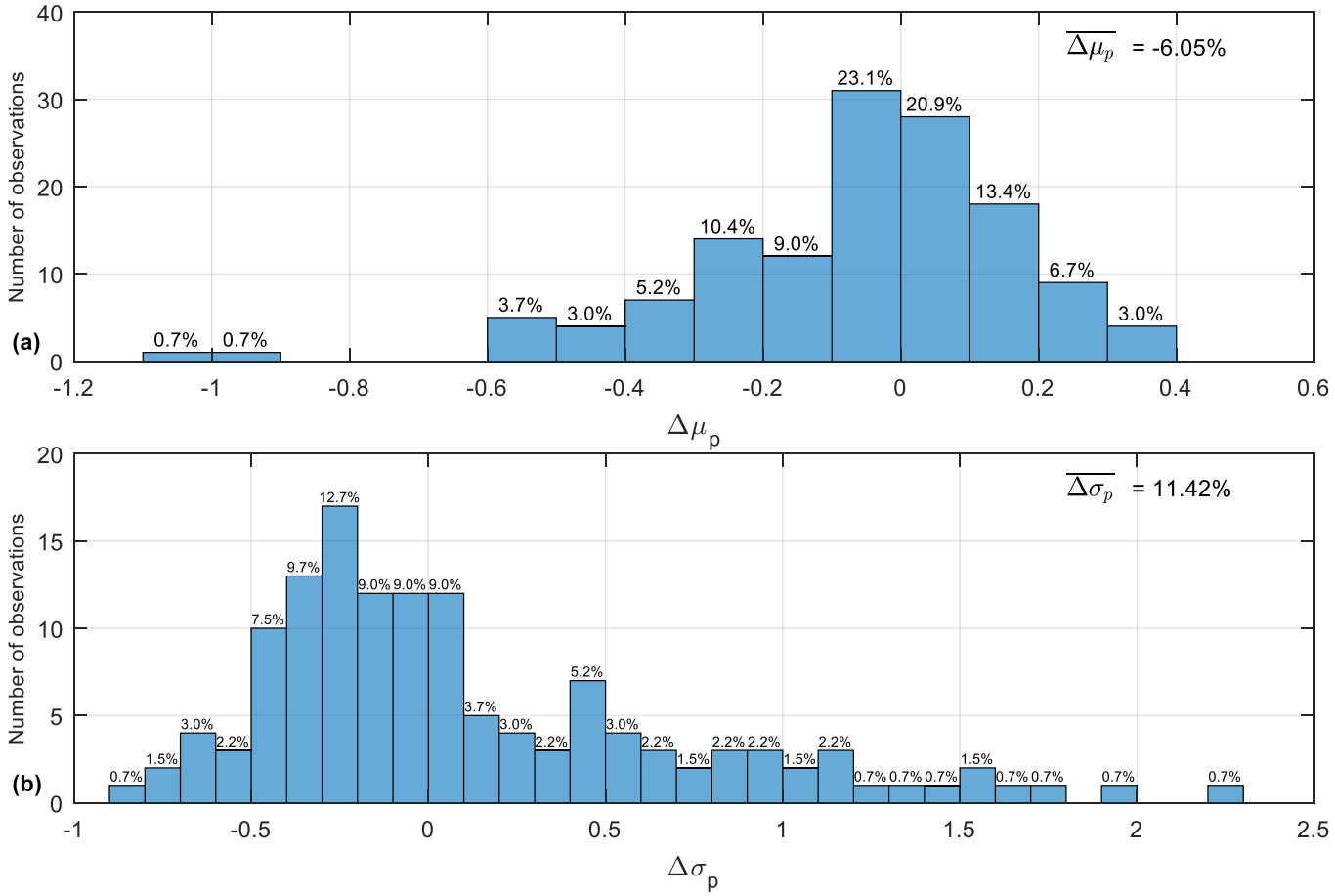

Fig. 9. Histogram of (a) mean and (b) standard deviation of the effective pressure difference (in decimal) between numerical simulations and experimental results.

6. CONCLUSION

To simulate non-simultaneous ice failure effects on ice-structure interaction, an extended model based on the previous work of Ji and Oterkus (2018) was developed. An assumption was made that the size of ice failure zone will decrease when ice velocity increases. Therefore, the ice failure length and width decreases, which increase the possibility of non-simultaneous effect on ice failure. Numerical results agree well with those in Sodhi (1998) and indicates that variations of ice force decrease with increasing ice velocity and increasing structural width, respectively. There is simultaneous failure occurrence on all segments at lower ice velocity, indicating large size of ice failure zone at ductile bending failure mode. At higher ice velocity, there is more random peak forces taking place on different segments, indicating more non-simultaneous ice failures at smaller brittle crushing zones. The simulation results from a series of 134 blind tests demonstrate the model's capability of predicting at different ice velocities, structural widths and ice thicknesses. In addition, analysis of the ice indentation experiments shows that the mean and minimum effective pressure have an approximately linear relationship with ice velocity which testified the assumption on variations of ice failure zone in the model.

ACKNOWLEDGEMENT

The first author would like to acknowledge the Mac Robertson Travel Scholarship provided by the University

of Glasgow and the University of Strathclyde for his visit to the University of Michigan.

REFERENCES

Ashby, M., Palmer, A., Thouless, M., Goodman, D., Howard, M., Hallam, S., Murrell, S., Jones, N., Sanderson, T., Ponter, A., 1986. Nonsimultaneous failure and ice loads on arctic structures, Offshore Technology Conference. Offshore Technology Conference.

Bhat, S., 1990. Modeling of size effect in ice mechanics using fractal concepts. Journal of Offshore Mechanics and Arctic Engineering 112 (4), 370-376.

Hendrikse, H., Kuiper, G., Metrikine, A., 2011. Ice induced vibrations of flexible offshore structures: the effect of load randomness, high ice velocities and higher structural modes, 21st International Conference on Port and Ocean Engineering Under Arctic Conditions, p. 031.

Huang, G., Liu, P., 2009. A dynamic model for ice-induced vibration of structures. Journal of Offshore Mechanics and Arctic Engineering 131 (1), 011501.

Ji, X., Oterkus, E., 2016. A dynamic ice-structure interaction model for ice-induced vibrations by using van der pol equation. Ocean Engineering 128, 147-152.

Ji, X., Oterkus, E., 2018. Physical mechanism of ice/structure interaction. Journal of Glaciology 64 (244), 197-207.

Johnston, M., Croasdale, K.R., Jordaan, I.J., 1998. Localized pressures during ice–structure interaction: relevance to design criteria. Cold Regions Science and Technology 27 (2), 105-117.

Karr, D.G., Troesch, A.W., Wingate, W.C., 1993. Nonlinear dynamic response of a simple ice-structure interaction model. Journal of Offshore Mechanics and Arctic Engineering 115 (4), 246-252.

Kry, P., 1978. A Statistical Prediction of Effective Ice Crushing Stresses on Wide Structure, Proc. of IAHR Ice Symposium.

Kry, P., 1980. Third Canadian geotechnical colloquium: Ice forces on wide structures. Canadian Geotechnical Journal 17 (1), 97-113.

Matlock, H., Dawkins, W.P., Panak, J.J., 1971. Analytical model for ice-structure interaction. Journal of the Engineering Mechanics Division 97 (4), 1083-1092.

Sodhi, D.S., 1991. Ice-structure interaction during indentation tests, in: Jones S., T.J., McKenna R.F., Jordaan I.J. (Ed.), Ice-Structure Interaction. Springer, Berlin, Heidelberg, pp. 619-640.

Sodhi, D.S., 1998. Nonsimultaneous crushing during edge indentation of freshwater ice sheets. Cold Regions Science and Technology 27 (3), 179-195.

Sodhi, D.S., Haehnel, R.B., 2003. Crushing ice forces on structures. Journal of Cold Regions Engineering 17 (4), 153-170.

Wang, L., Xu, J., 1991. Description of dynamic ice-structure interaction and the ice force oscillator model, 11 th International Conference on Port and Ocean Engineering under Arctic Conditions, St. John's, Canada, pp. 141-154.

Withalm, M., Hoffmann, N., 2010. Simulation of full-scale ice–structure-interaction by an extended Matlock-model. Cold Regions Science and Technology 60 (2), 130-136.

Yu, B., Karr, D., 2014. An ice-structure interaction model for non-simultaneous ice failure, OTC Arctic Technology Conference. Offshore Technology Conference, p. 24547.

Yue, Q., Guo, F., Kärnä, T., 2009. Dynamic ice forces of slender vertical structures due to ice crushing. Cold Regions Science and Technology 56 (2), 77-83.